International Journal of Biological Macromolecules 245 (2023) 125516

Contents lists available at ScienceDirect

International Journal of Biological Macromolecules

journal homepage: www.elsevier.com/locate/ijbiomac

An evaluation of antibacterial properties and cytotoxicity of UV-curable biocompatible films containing hydroxyethyl cellulose and silver nanoparticles

Yusuf Özdemir [a], Hatice Birtane [b], Aslı Beyler-Çiğil [c,*]

[a] Institute of Science, Department of Chemistry, Amasya University, Amasya, Türkiye
[b] Department of Chemistry, Marmara University, İstanbul, Türkiye
[c] Department of Chemistry and Chemical Process Technology, Gazi University, Ankara, Türkiye

ARTICLE INFO

Keywords:
Cellulose
Ag nanoparticles
Thiol-ene click
Antibacterial properties
Anticancer properties

ABSTRACT

The present study aimed to develop biocompatible film materials with antibacterial and anticancer properties that can be cured with UV rays depending on the thiol-en click reaction mechanism. The synthesized m-Ag NPs were added to formulations containing acrylate functionality HEC, pentaerythritol tetrarkis(3-mercaptopropionate), and photoinitiator at different rates (0, 20, 40, and 60 parts per hundred (phr)). The antibacterial activity of the films was evaluated against *S. aureus, P. aeruginosa* and *E. coli* by the disk diffusion test. The antibacterial effect of the films did not form an inhibition zone for the control formulation (Cm-Ag0) against bacteria whereas the antibacterial property increased as the Ag NPs content increased in formulations containing m-Ag NPs. The strongest resistance film against the three bacterial species was observed in the Cm-Ag60 formulation with 60 phr silver content, and the inhibition zones for *S. aureus*, *P. aeruginosa*, and *E. coli* were measured as 16.5 ± 0.7, 16.5 ± 2.1, and 16 ± 1.4, respectively. The cytotoxicity of the films against healthy cells and breast cancer cell (MCF-7) lines was investigated with MTT, and it was observed that all films did not cause any inhibition in the structure of the living cell but killed the cells at a high rate in the MCF-7 line. It was mainly observed that the Cm-Ag60 formulation showed 95.576 % cell inhibition against MCF-7. According to these results, it has been predicted that the prepared films will play a vital role in the next generation of cancer treatments.

1. Introduction

Cancer is regarded as the disease of the century and is the second leading cause of death in humans after cardiovascular diseases. Cancer is rising due to significantly increased risk factors such as a sedentary lifestyle, population aging, tobacco, and malnutrition. Current conventional therapies using synthetic generic drugs, hormone therapy, chemotherapy, surgery, and radiation therapy are proving to be inadequate in the treatment of cancer [1–3]. Also, microbial infections have become important health issues, especially in developing countries. Many different approaches have been developed over time against these microbial infections. Among these, the preparation of systems containing antibacterial agents such as antibiotics, nanoparticles, and quaternary salts (ammonium, phosphonium or sulfonium) has become critical. Antibiotics are among these agents and often cause antibiotic resistance in repeated use, rendering the drugs ineffective [4–6]. Therefore, new studies are required to search for new materials/agents that are inexpensive and effective treating of these diseases. Recent research has focused on producing nanocomposites prepared with natural biopolymers and metal nanoparticles using materials with potential alternative antimicrobial and anticancer properties.

Silver nanoparticles (Ag NPs) refer to silver clusters with particle size in the range of 1–100 nm, with a large specific surface area, and possess sound inhibitory effects against Gram-positive and Gram-negative bacteria and fungi [7–9]. Silver nanoparticles with different particle sizes show various toxic effects on bacteria. The widely recognized antibacterial mechanisms of Ag NPs comprise disrupting the normal function of the cell wall, interfering with the normal function of the cell membrane by interacting with the lipid components, inducing ROS free radicals to damage the cell membrane, damaging the DNA structure, and inhibiting

* Corresponding author.
E-mail address: asli.beyler@gazi.edu.tr (A. Beyler-Çiğil).

https://doi.org/10.1016/j.ijbiomac.2023.125516
Received 27 January 2023; Received in revised form 6 June 2023; Accepted 20 June 2023
Available online 22 June 2023
0141-8130/© 2023 Elsevier B.V. All rights reserved.

a bonding of with enzyme proteins with sulfhydryl groups to inactive the cell [10–12]. Ag NPs is an antibacterial agents added to ceramics, films, coatings, and textile materials due to their simple preparation methods and broad-spectrum antibacterial properties. However, in most studies, multi-directional and dispersed particles are produced, making it difficult to obtain stable colloidal systems, and often inconsistent results. These antibacterial agents also migrate from the material over time and adversely affect the properties of the material. However, the use of inorganic nanoparticles in polymeric films requires attention due to the weak interfacial interaction between nanoparticles and polymer matrix and their tendency to form aggregates and agglomerates in polymeric films. Surface modifiers are widely used to improve compatibility between nanoparticles and polymer matrices in composite films [13–15].

Organosilanes can be utilized as an effective surface modifier for inorganic nanoparticles with the general chemical structure of $(RO)_3SiX$. These chemicals include hydrolyzable alkoxys (RO) such as methoxy and ethoxy and an organofunctional group (X) such as methyl, vinyl, and methacrylate groups. The silanization of inorganic fillers usually occurs in two stages, hydrolysis and condensation *via* sol-gel. Surface-modified inorganic nanoparticles can both disperse more homogeneously on the surface and covalently bind to the polymeric matrix as they are modified with the desired functional group [14,16–18].

In recent years, materials chemistry trends have shifted towards using bio-based materials derived from renewable and sustainable sources due to the depletion of oil reserves and carbon footprint issues [19,20]. Cellulose derivatives have great potential due to their biocompatible, environmentally-friendly, low-cost, easy-to-access, and easy-film-forming abilities. They are biocompatible and biodegradable due to the nature of production from living organisms. Cellulose molecules have active hydroxyl groups that can combine them with other polymers, inorganics, organics, and nanomaterials [21–23].

In the literature, there are studies on composites prepared for different purposes from cellulose and Ag NPs. In a study conducted in 2022, chitosan/carboxymethyl cellulose wound dressing material supplemented with biologically synthesized silver nanoparticles was obtained from the Ligninolytic fungus Anamorphous *Bjerkandera* s R_1 [24]. In another study conducted in 2020, carboxymethyl cellulose/cellulose nanocrystals were immobilized to silver nanoparticles as an effective coating to improve the barrier and antibacterial properties of paper for food packaging applications [25]. Also, another study obtained carboxymethyl cellulose-ε-polylysine hybrids containing magnetic self-assembled silver nanoparticles with synergistic antibacterial activity for wound infection treatment [26]. Again in 2022, biodegradable antibacterial coatings were prepared with covalently bonded nanosilver-hydroxyethyl cellulose/sorbitol [27].

Thiol-en photocured-initiated radical polymerization has significantly progressed recently [28,29]. This was mainly associated with the rapid cure at a relatively low temperature with low emissions of volatile organic compounds, allowing films prepared by thiol-ene photocuring to be more environmentally friendly and attractive. Films prepared from thiol-en photocurable monomers have recently become popular due to their fast-curing rates, energy efficiency, and high dimensional stability [30–32].

To our knowledge, there are no studies on biocompatible films with antibacterial and anticancer effects, containing cellulose and Ag NPs prepared by thiol-ene photopolymerization. Accordingly, HEC was reacted with isocyanate ethyl methacrylate to gain acrylate functionality, and FTIR investigated its functional groups. Then, silver nanoparticles were synthesized acrylate functionality was added to the synthesized silver nanoparticles in the presence of organosilane compounds, and FTIR investigated their functional groups. The synthesized m-Ag NPs were added to formulations containing acrylate functionality HEC, 4-SH and photoinitiator at 0, 20, 40, and 60 phr. The prepared formulations were cured with UV rays, and biocompatible film materials were developed with a simple and environmentally friendly method. DLS measured size analyses of prepared Ag NPs and m-Ag NPs. SEM characterized the morphological properties of the prepared biocompatible films, and SEM-EDAX characterized the elemental compositions. The disk diffusion test against *E. coli*, *P. aeruginosa*, and *S. aureus* bacteria evaluated the antibacterial effect of the films. Also, the cytotoxic effects of the films were determined by the MTT test using the breast cancer cell line (MCF-7) and healthy cell line (VETO).

2. Materials and methods

2.1. Materials

Silver nitrate, sodium borohydride, polyvinylpyrrolidone (PVP), glycerol, hydroxyethyl cellulose (HEC), 2-butanone (MEK), dibutyltin dilaurate (DBTDL), 2-Isocyanatoethyl methacrylate (IEM), (3-mercaptopropyl) trimethoxysilane (MPTS), 3-(trimethoxysilyl)propyl acrylate (APTMS), pentaerythritol tetrakis (3-mercaptopropionate) (4-SH) and 1-Hydroxycyclohexyl phenyl ketone (Irg 184) were obtained from Sigma Aldrich company.

2.2. Synthesis of Ag NPs

Silver nanoparticles were prepared similarly to previous studies in the literature [33]. Accordingly, aqueous solutions were prepared by dissolving $AgNO_3$ (0,1 M), $NaBH_4$ (0,01 M), and PVP (0,01 M) in deionized water. Then, the aqueous solutions of 100 mL of PVP and 100 mL of $NaBH_4$ were mixed and 50 mL of $AgNO_3$ solution was added slowly. As $AgNO_3$ was slowly added to the colorless solution of $NaBH_4$ and PVP, the color of the solution began to change from yellow to pale brown, indicating the formation of silver nanoparticles. A 4 mL of glycerol was added to the resulting silver nanoparticle solution and the mixture was stirred at room temperature for 15 min using a magnetic stirrer.

2.3. Modification of Ag NPs (m-Ag NPs)

(3-Mercaptopropyl)trimethoxysilane (MPTS) and 3-(trimethoxysilyl)propyl acrylate (APTMS) solutions were prepared by the sol-gel method. A solution containing 5 g of APTMS and ethanol was prepared, then the amount of APTMS was adjusted to 50 wt% compared to the solution and the solution was stirred until becoming completely homogeneous, and then 0.2 g of MPTS was added. The resulting solution was continuously stirred for an additional 30 min. Then, 50/50 aqueous hydrochloric acid solution (pH:1) and ethanol were prepared and added. The hydrolyzed solution was stirred for 3 h on a magnetic stirrer and left at room temperature for 24 h. Then, 5 % Ag NPs were added to 10 mL of the prepared MPTS and APTMS mixture. The solution was dispersed in an ultrasonic bath for 30 min. As a result, Ag NPs entrapped in MPTS and APTMS were obtained. The schematic representation of the modification is given in Fig. 1.

2.4. Modification of hydroxyethyl cellulose

Acrylate modification of hydroxyethyl cellulose was carried out similarly to the previous synthesis in the literature [34]. Accordingly, 5 g of HEC was dissolved in 50 mL of dry 2-butanone (MEK) until the solution became homogeneous, and then the solution was taken into a 250 mL three-necked flask. The system containing nitrogen inlet, reflux, and dropping funnel was dried with a flame until the moisture in the system was completely removed from the environment. Dibutyltin dilaurate (DBTDL) (0.1 wt%) (as the catalyst) was added to the reaction flask and the system was heated to 50 °C. In a separate beaker, IEM equivalent to 50 wt% of the theoretical hydroxyl content of HEC was taken, dissolved in dry MEK, and added dropwise to the flask being stirred at 500 rpm on a magnetic stirrer. The FTIR hourly-taken spectrum results controlled the decrease and disappearance of the -NCO peak. With the disappearance of the -NCO peak, it was confirmed that the reaction was complete,

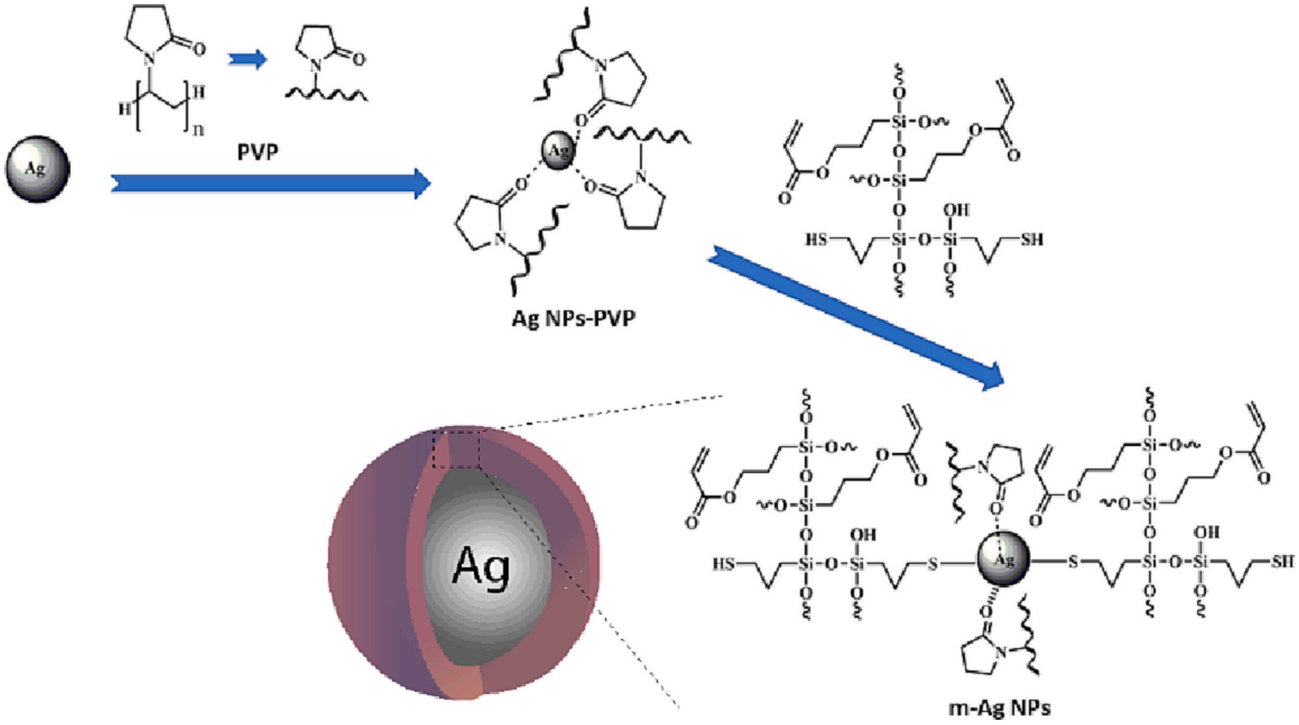

Fig. 1. Modification of Ag NPs (m-Ag NPs).

and the resulting resin was precipitated in excess methanol, then filtered and dried in a vacuum oven. The modification of hydroxyethyl cellulose is given in Fig. 2.

2.5. Preparation of biocompatible films

The thiol-en-click reaction mechanism in the presence of UV rays prepared biocompatible film materials. The contents of the prepared formulations are given in Table 1.

Except for the photoinitiator, the other monomers were weighed in a clean beaker wrapped in aluminum foil in the amounts specified in Table 1 and homogenized in the homogenizer. Then, 3 %-by-weight 1-hydroxycyclohexyphenylketone (Irg184, photoinitiator) was added, and the homogeneous formulations obtained to obtain a free film were poured into Teflon® molds (10 × 20 × 1 mm) and cured under UV light (OSRAM, λ_{max} = 365 nm, 10 mW/cm^2) for 3 min. 3 min is generally enough for typical UV-curable thiol-ene systems to ensure that a high crosslinking degree is achieved. At the end of this period, the absence of a drop of monomer residue on the surface indicates that the reaction was completed. All the free films prepared were made ready for characterizations. The preparation of biocompatible films is given in Fig. 3.

2.6. Characterization

Functional group analyses of synthesized cellulose acrylate and Ag nanoparticles with acrylate functionality were performed with the Perkin-Elmer Spectrum 100 FTIR spectrophotometer. Spectra were recorded in the wavenumber range of 380–4000 cm^{-1}.

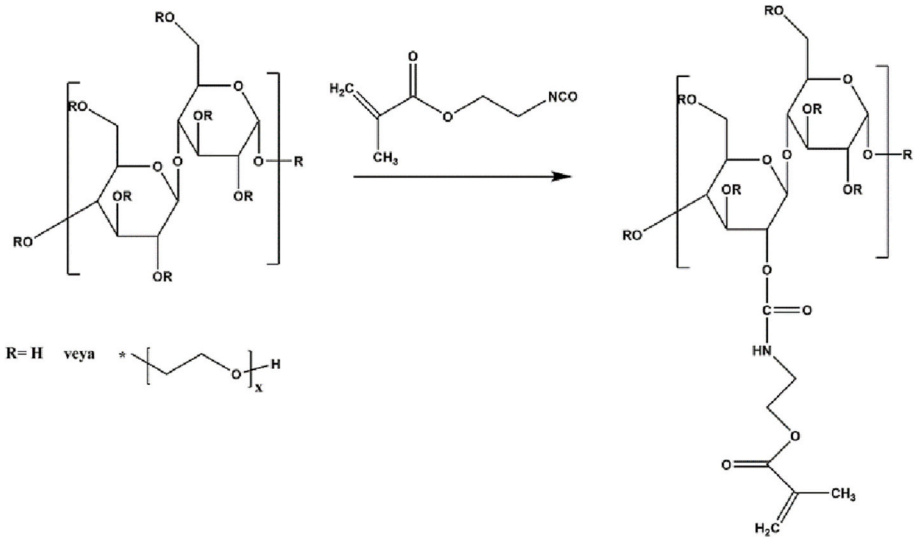

Fig. 2. Modification of hydroxyethyl cellulose.

Table 1
Formulations of biocompatible films.

	Acrylate group modified HEC (%)	Pentaerythritol tetrakis (3-mercaptopropionate) (4-SH)	Irg 184 (phr)	m-Ag NPs (phr)
Cm-Ag0	60	40	3	–
Cm-Ag20	60	40	3	20
Cm-Ag40	60	40	3	40
Cm-Ag60	60	40	3	60

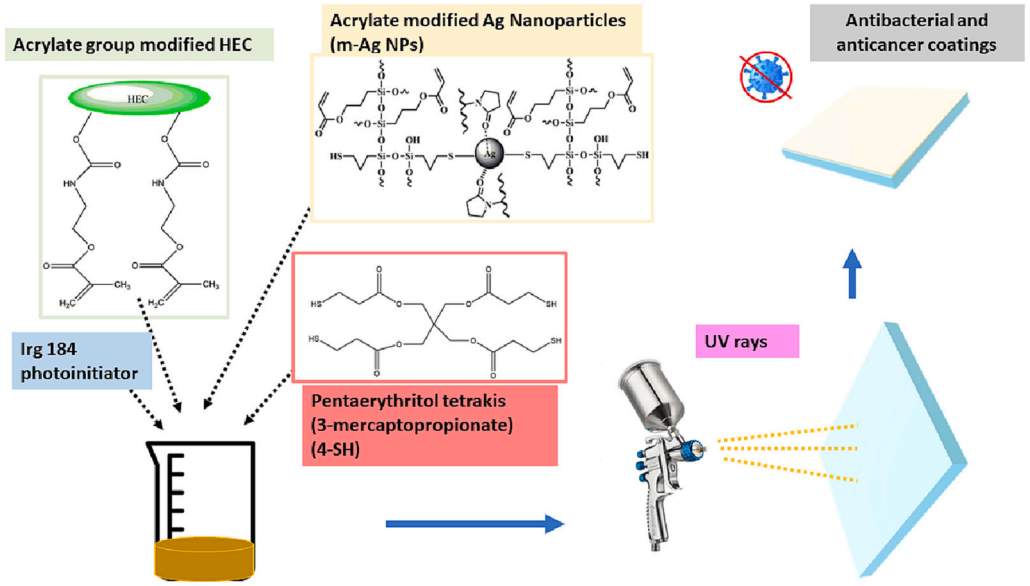

Fig. 3. Preparation of biocompatible films.

The EXSTAR SII 7300 model Thermogravimetric Analysis/Differential Thermal Analysis (TGA/DTA) device was used to measure the thermo-oxidative stability of the prepared biocompatible films. The measurements were carried out in nitrogen atmospheres with a heating rate of 20 °C/min, between 30 °C–750 °C (Amasya University).

The fracture surface morphology of the prepared biocompatible films, the distribution of silver nanoparticles on the surface, and the chemical composition of the films were investigated by SEM-EDAX using the PhillipsXL 30 ESEM-FEG/EDAX microscope. For imaging in SEM, biocompatible films were fractured in liquid nitrogen, the fractured surface was covered with a thin layer of platinum, and imaging was performed (Bogazici University).

The size analysis of the obtained Ag nanoparticles was measured with Nano-PSA/Zeta (Brookhaven 90Plus Nano Particle Size/Zeta Potential Analyzer). The measurements were carried out using the Laser Dynamic Beam Scattering Technique (DLS) used for suspended particles in the 2 nm-3 μm range with a powerful 35 mW laser. Before the measurement, 10 % Ag NPs and m-Ag NPs were mixed in a sonicator for 60 min and then the measurements were carried out (Bogazici University).

The susceptibility of biocompatible films to bacteria was performed on the MH agar by the Kirby–Bauer disk diffusion technique, considering the recommendations of CLSI January-2011 documents M02 and M07. Sterile, disposable, MH agar with a 4-mm-high medium was used on Petri dishes with a diameter of 15 cm. Bacterial colonies that developed new as pure colonies on the culture dishes were collected with a sterile loop, and inoculated into MH broth, incubated for 1–2 h at 37 °C. After the formation of turbidity, standard turbidity was created by adjusting to McFarland 0.5 (10^8 microorganisms/mL). Widespread cultivation was performed from this suspension on MH agar medium with a sterile swab. All prepared biocompatible films were placed in small pieces directly into the culture media with sterile forceps. Similarly, a control formulation with no silver nanoparticles was prepared (Cm-Ag0). Three different antibiotics were used for control purposes. The Petri dishes were incubated at 35–37 °C for 18–24 h. The diameter of the zone of inhibition around the films was measured by examining the bacterial growth in Petri dishes (Amasya University).

The anticancer effects of prepared biocompatible films on breast cancer cells were examined by the methyl thiazole tetrazolium (MTT) test. To determine the anticancer effect using the MTT method, three replications were conducted in 12 wells of a 96-plate and 1×10^4 MCF-7 cells in 100 μl for each well. After seeding, cells were incubated for 24 h. Then, 1-mm-cut biocompatible films (Cm-Ag0, Cm-Ag20, Cm-Ag40 ve Cm-Ag60) were added to the wells. Also, negative control and a DMSO control group were used. To examine the effect of the doses, MTT (100 μl per well) solution was added to the cells that were incubated in an oven for 24 h and incubated for 3 h. At the end of this period, the MTT solution was removed from the wells and the reaction was terminated with DMSO. Measurements were carried out with a spectrophotometer at a wavelength of 570 nm. % cell viability values were determined by concentration-absorbance graph (Amasya University).

The cytocompatibility of the prepared antibacterial films on fibroblast cells was similarly studied by examining the anticancer effects described above. Healthy cells (VERO) were used instead of MCF-7.

3. Results and discussion

3.1. Characterizations of m-Ag NPs

3.1.1. FTIR spectroscopy

MPTS and APTMS solutions were prepared by the sol-gel method and silver nanoparticles were added to this prepared solution. As a result, Ag NPs imprisoned in MPTS and APTMS, with acrylate functionality, were prepared. The functional groups of Ag NPs and Ag NPs after acrylate modification were examined by FTIR spectroscopy and are given in

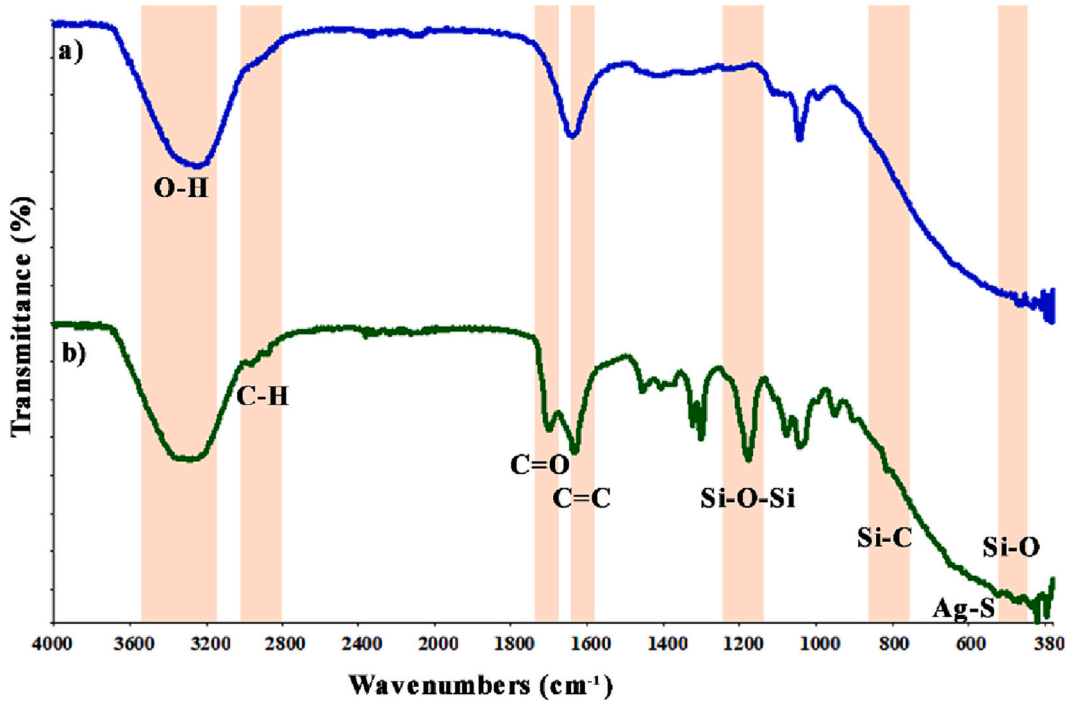

Fig. 4. FTIR spectrum of a) Ag NPs-PVP, and b) m-Ag NPs.

Fig. 4.

Examining the spectra of Ag NPs and m-Ag NPs, some PVP-related peaks are seen in the FTIR spectrum of unmodified Ag NPs due to the stabilization of Ag NPs with polyvinylpyrrolidone (PVP). It was seen that the stretching vibration band of the O-H bond observed at 3341 cm^{-1} in the spectrum. The peaks observed in the spectrum at 2854 and 2923 cm^{-1} were due to the asymmetric stretching of the C-H bond in the methacrylate groups in the organosilane group and the vinyl pyrrolidone groups in the PVP. After modification, the increase in these peaks indicated that the organosilane was bound on the Ag NPs' surface. Also, the peaks at 1180, 800, and 450 cm^{-1} that appear after modification was associated with the asymmetric stretching of Si-O-Si bonds, symmetrical stretching of Si-O-Si bonds, and bending vibration of Si-O-Si bonds, respectively. The peak around 1650 cm^{-1} in Fig. 4.1a can be attributed to the stretch of C═O (carbonyl in the PVP group). The increase in this peak after modification is due to the presence of the carbonyl group in the methacrylate in the organosilane group. All observed peaks were compatible with the literature [14,35–38]. Also, the absence of peaks attributed to the S-H bond in (3-mercaptopropyl)trimethoxysilane, which is expected to be seen at 2560 cm^{-1} and 2524 cm^{-1}, reveals the efficient interaction of SHs with the surface of Ag NPs (Ag-S) [39]. Finally, the peaks at 1642 $cm^{-1,}$ which are not seen in the spectrum of Ag NPs and seen in the spectra of m-Ag NPs, originate from C═C vibrations [40]. The obtained results, show that acrylate groups were successfully modified on the surface of Ag NPs.

3.1.2. Size analysis

The size distributions of synthesized Ag NPs and m-Ag NPs are shown in Supplementary Fig. 1. The average particle size for Ag NPs was measured as 6.2 ± 0.6 nm. Ag NPs synthesized by various methods in various sizes are found in the literature. For example, in 2020, Chen et al. prepared Ag NPs from silver nitrate using *N*,*N*-dimethylacetamide (DMAc) as a reducing agent in the presence of PVP. The researchers have reported that the size of 90.79 % of the Ag NPs they prepared after 1 h of reaction was approximately between 3 and 8 nm [7]. Small-sized Ag NPs tend to agglomerate rapidly. However, the lack of agglomeration in the DLS results shows that PVP used as a surfactant effectively prevents the rapid agglomeration of Ag NPs. Thus, it is seen that the size of Ag NPs has a specific range and narrow distribution. Das et al. [41] showed that trisodium citrate (TSC) represented an effective way to control the size and size distribution in the synthesis of Ag NPs in the presence of the stabilizing agent. The researchers observed that the size of the synthesized Ag NPs changed by varying the concentration of the stabilizing agent. DLS results in the mentioned study showed that the particle size decreased to a minimum value with increasing TSC concentration, but then the particle size increased again. Therefore, the researchers have reported the importance of optimizing the stabilizing agent concentration to achieve the minimum particle size with narrow size distribution. The concentration of the stabilizing agent varied in different experimental studies, yielding stable particles with an average size of 7 nm and narrow size distribution [41]. In the present study, the average particle size for Ag NPs was measured as 6.2 ± 0.6 nm in the presence of a PVP stabilizing agent. It is understood from the comparisons that the prepared Ag NPs were compatible with the literature.

However, after treatment with MPTS and APTMS, the size of Ag NPs increased noticeably. The average particle size for the Ag NPs after acrylate modification was measured to be 27.8 ± 0.4 nm. This increase showed that adding organosilane groups leads to an increase in the core size. Khalkho et al. synthesized Ag NPs with an average particle size of 8 nm and modified the synthesized Ag NPs with L-cysteine (Cys). DLS measured the average particle size of Cys-modified-Ag NPs as 57.8 ± 6.4 nm [42]. In another study, Solyman et al. prepared Fe, Ag/Fe, APTES-Ag/Fe, and PEI-Ag/Fe nanoparticles. The researchers have stated that the iron oxide NPs prepared by DLS had an average particle size of 39 nm with a narrow distribution. The researchers have also mentioned that this value increased with the addition of Ag NPs and the addition of APTES-Ag and PEI-Ag NPs to the Fe surface. Average particle sizes for Ag/Fe, APTES-Ag/Fe, and PEI-Ag/Fe were reported as 195.8 nm, 295.3 nm, and 283.5 nm, respectively [43].

3.2. Structural characterization of acrylate-modified hydroxyethyl cellulose

3.2.1. FTIR spectroscopy

Structural characterizations of HEC, HEC modified with acrylate groups, and IEM were examined by FTIR spectroscopy and are shown in

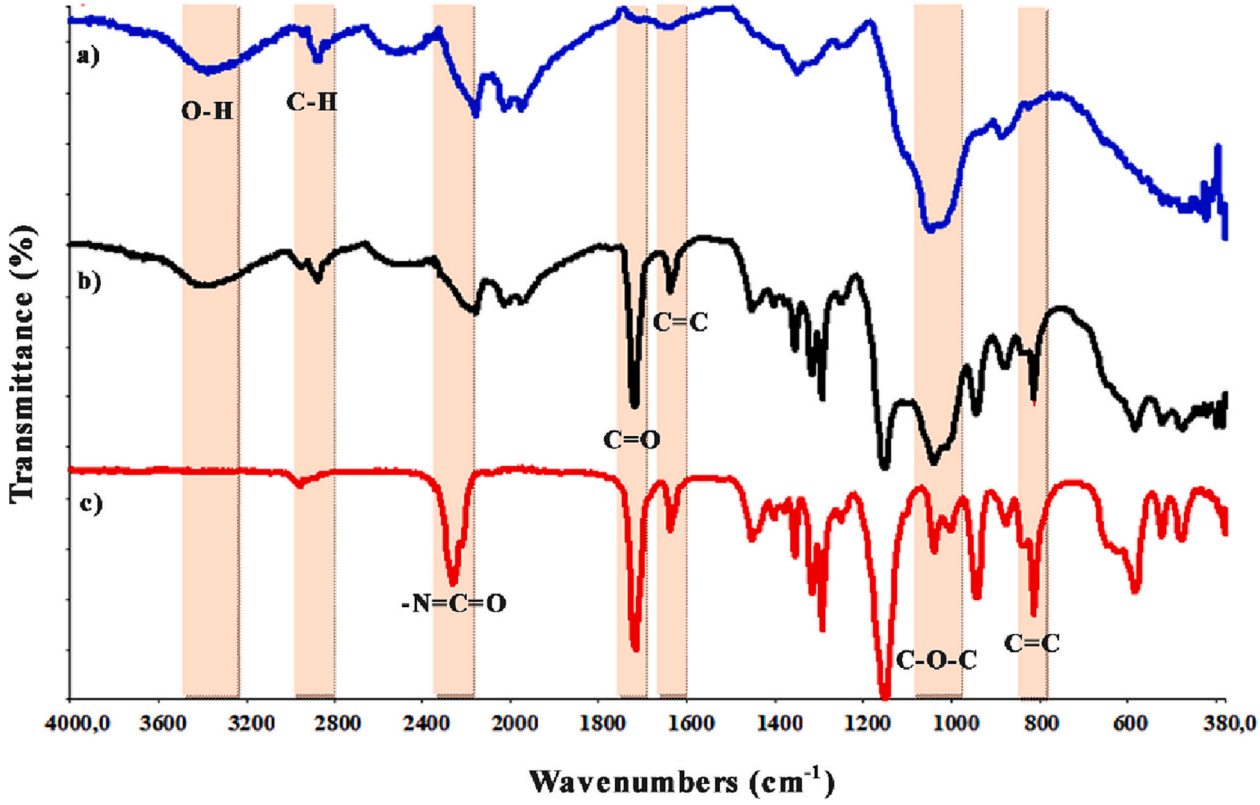

Fig. 5. FTIR spectrum of a) HEC, b) acrylate-modified hydroxyethyl cellulose, and c) IEM.

Fig. 5. Examining the FTIR spectrum of HEC in Fig. 5, the peaks seen at 2880 cm^{-1} were associated with the characteristic absorption peaks of methylene belonging to ethyls in hydroxyethyl cellulose. Also, the stretching vibration of C-O-C bonds of the polysaccharide skeleton at 1028 cm^{-1}, characteristic peaks of the β-1,4-glycosidic bond at 1153 and 895 cm^{-1} and peaks related to the stretching vibration of hydroxyl groups (-OH) at 3400 cm^{-1} was observed. In the spectrum taken after the reaction with 2-isocyanatoethyl methacrylate, in addition to the overlap in other peaks, the new peak at approximately 1750 cm^{-1} represents the stretching vibrations of the carbonyl groups (C=O) of the esters in the IEM structure. The absence of the absorption band at 2275 cm^{-1}, which is bound to the characteristic isocyanate group in IEM, indicated the reaction between IEM and HEC. Also, it was seen that the peaks of the vibrations of the C=C bonds in the acrylate structure at 1635 and 810 cm^{-1} become more pronounced.

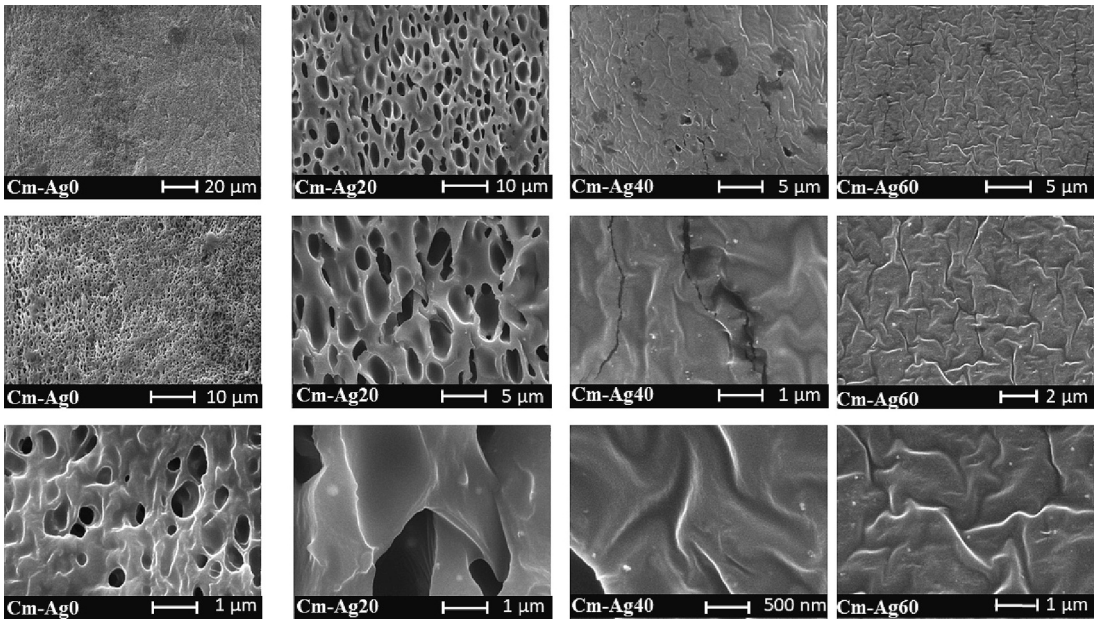

Fig. 6. SEM images of biocompatible films.

3.3. Examination of the surface properties of biocompatible films

SEM images of the fractured surface of the prepared Cm-Ag0, Cm-Ag20, Cm-Ag40, and Cm-Ag60 biocompatible films are given in Fig. 6. Also, the percentile composition of the elements in the films was characterized by the EDAX analysis and is given in Fig. 7.

Examining the SEM image of the control film formulation Cm-Ag0, it was seen that the surface is homogeneous and smooth. The presence of Ag NPs was seen in other formulations. Nanocomposite films containing nanosized particles are of great interest in developing high-performance films. However, the use of inorganic nanoparticles in polymeric films requires attention due to the weak interfacial interaction between nanoparticles and polymer matrix and their tendency to aggregate and agglomerate in polymeric films [44,45]. Organosilanes are widely used as surface-modifying chemicals in composite films to increase compatibility between nanoparticles and polymer matrices. Examining Fig. 6, it was seen that the nanoparticles are homogeneously dispersed in the polymeric matrix with the addition of nanoparticles [14]. In the present study, the modification of MPTS and APTMS organosilane compounds and Ag NPs was carried out to covalently bind nanoparticles to the polymeric matrix and create compatibility with the polymeric matrix. Examining Fig. 6, it is seen that the nanoparticles are homogeneously dispersed in the polymeric matrix with the addition of nanoparticles (white dots). In the literature, corrosion-resistant coatings have been prepared by adding Ag NPs, the surface of which has been modified with 3-methoxy propyl methacrylate, to the epoxy matrix. Examining the SEM analyses of the prepared coatings, it has been reported that the surface-modified Ag NPs were more homogeneously dispersed in the epoxy matrix than the unmodified nanoparticles [14]. The researchers have mentioned that the nanoparticles without surface modification were not homogeneously dispersed due to agglomeration.

Examining the EDAX results in Fig. 7, the presence of C, N, S, and O elements was seen in the Cm-Ag0 formulation, as expected. In other biocompatible films with added m-Ag NPs, different from these elements, Ag and Si elements were found as expected. As the percentage of m-Ag-NPs added to the biocompatible films increased, it was seen that the levels of Ag and Si elements in the compositions increased This proved that the modification was carried out successfully.

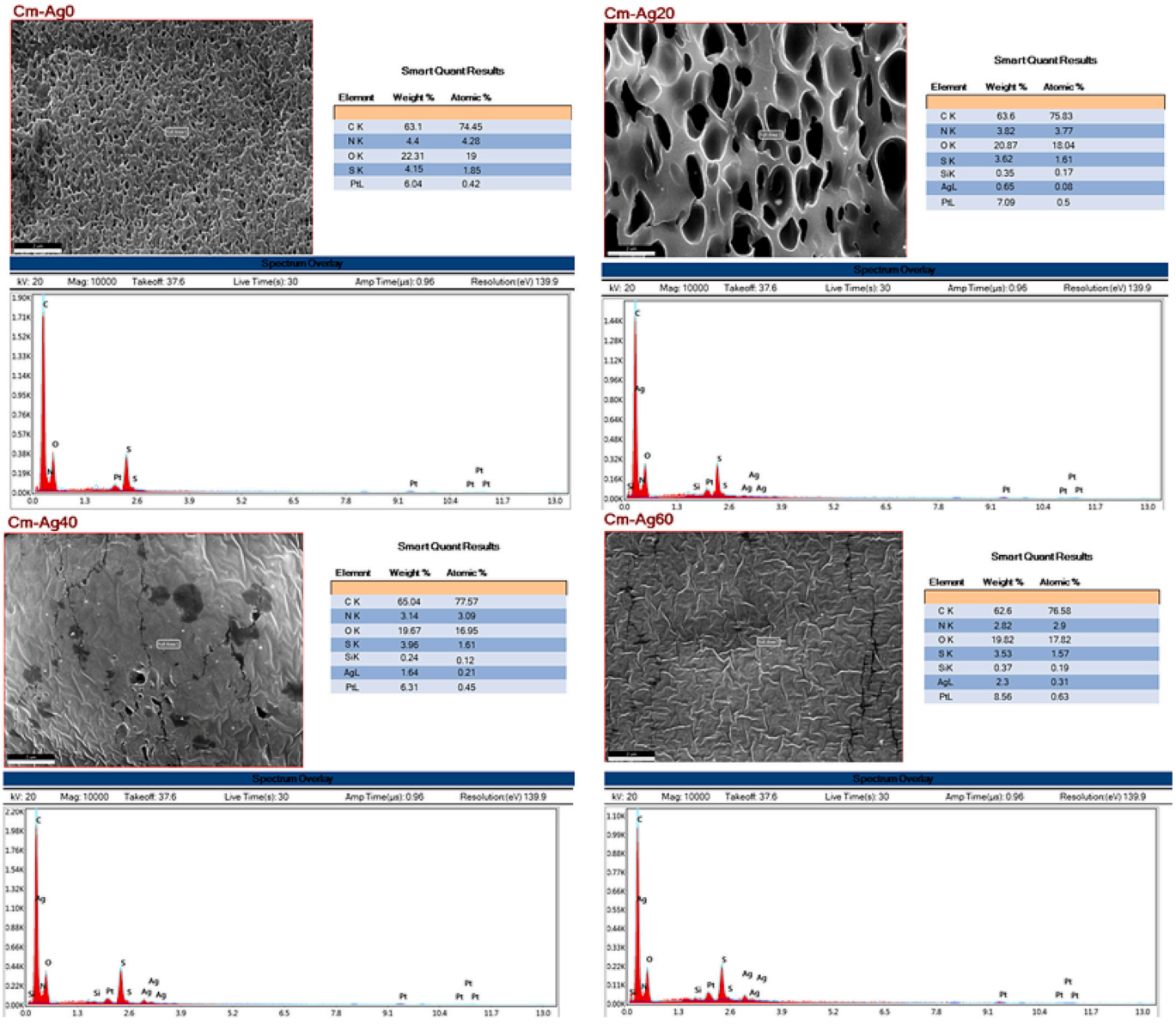

Fig. 7. SEM-EDAX results of biocompatible films.

3.4. Thermal properties of biocompatible films

The thermal stability of all prepared biocompatible films (Cm-Ag0, Cm-Ag20, Cm-Ag40, and Cm-Ag60) was investigated by TGA. TGA spectra of all films are given in Fig. 8. The maximum weight loss temperatures determined from the maximum of the corresponding derivative curves and the char yields at 750 °C are given in Table 2. In Fig. 8, it is seen that the weight loss of all films took place in two stages. The initial weight reduction in the 30–200 °C temperature range was probably due to the release of water from the cellulosic films. The second weight-loss stage occurred at 225–500 °C. The weight loss values at this stage are thought to result from the degradation of the polymeric structure. From the TGA curves, it was seen that the addition of Ag NPs surface modified with organosilane compounds to the films created an improvement in thermal stability and shifted the maximum decomposition temperatures of the films to higher temperatures, from which it can be concluded that the thermal strength of films containing Ag NPs was higher. However, it can be concluded that the increase in the m-Ag NPs did not cause a significant change. In a previous study, new hydrogels based on hydroxyethyl cellulose cross-linked with tungsten oxide-reinforced citric acid were developed for wound treatment [46]. Thermograms of cross-linked hydrogels, the thermal properties examined by TGA, agreed with the thermograms of films cross-linked with pentaerythritol tetrakis(3-mercapto propionate) prepared in the present study. In another study, Ali et al. prepared Ag NPs impregnated cellulose composites that can be used effectively in wound dressings and filtration for wastewater treatment to prevent bacterial attack at the wound site. The TGA thermograms of the prepared composites, showed that the main decrease in mass occurred around 300–400 °C [47]. The biocompatible films prepared in the present study were consistent with the temperature range where the primary decrease in mass was experienced.

Table 2
TGA analysis results of biocompatible films in nitrogen atmosphere.

	T_5[a] (°C)	T_{10}[a] (°C)	T_{max}[b] (°C)	Char yield (%)
Cm-Ag0	71	101	178/402	12
Cm-Ag20	84	119	190/428	9
Cm-Ag40	94	138	241/433	13
Cm-Ag60	95	144	241/431	11

[a] T_5 is the first 5 % weight loss temperature, and T_{10} is the first 10 % weight loss temperature, which are obtained from the corresponding derivative curves.
[b] T_{max} is the maximum weight loss temperature, which was determined from the maximum of the corresponding derivative curves.

3.5. Antibacterial properties of biocompatible films

The antibacterial activities of the prepared films were determined by the *E. coli*, *P. aeroginosa*, and *S. aureus* bacteria and were measured by examining the diameters of the inhibition zone using the disk diffusion method. The mean diameters of the inhibition areas are given in mm. The results are given in Table 3 and the inhibition area images are given in Fig. 9.

According to these results, the Cm-Ag0 formulation did not create an inhibition area for *E. coli*, *P. aeruginosa*, and *S. aureus*. The increased levels of m-Ag NPs in the formulations appeared to increase the area of inhibition against bacteria. The areas of inhibition against *S. aureus* bacteria of formulations with m-Ag NPs contents of 20, 40, and 60 phr were measured at 10 ± 1.41, 14 ± 1.41, and 16.5 ± 0.70 mm, respectively. This increase was seen against all bacteria. In a different study in the literature, cellulose nanofibers (CNF)/polyvinyl alcohol (PVA) composites containing different ratios of Ag NPs (1, 10 and 20 wt%) were prepared and the antibacterial activity of CNF/PVA, Ag NPs, CNF/PVA-Ag composite films was measured against two different Gram-negative (*E. coli*) and Gram-positive (*B. subtilis*) bacteria using the disk

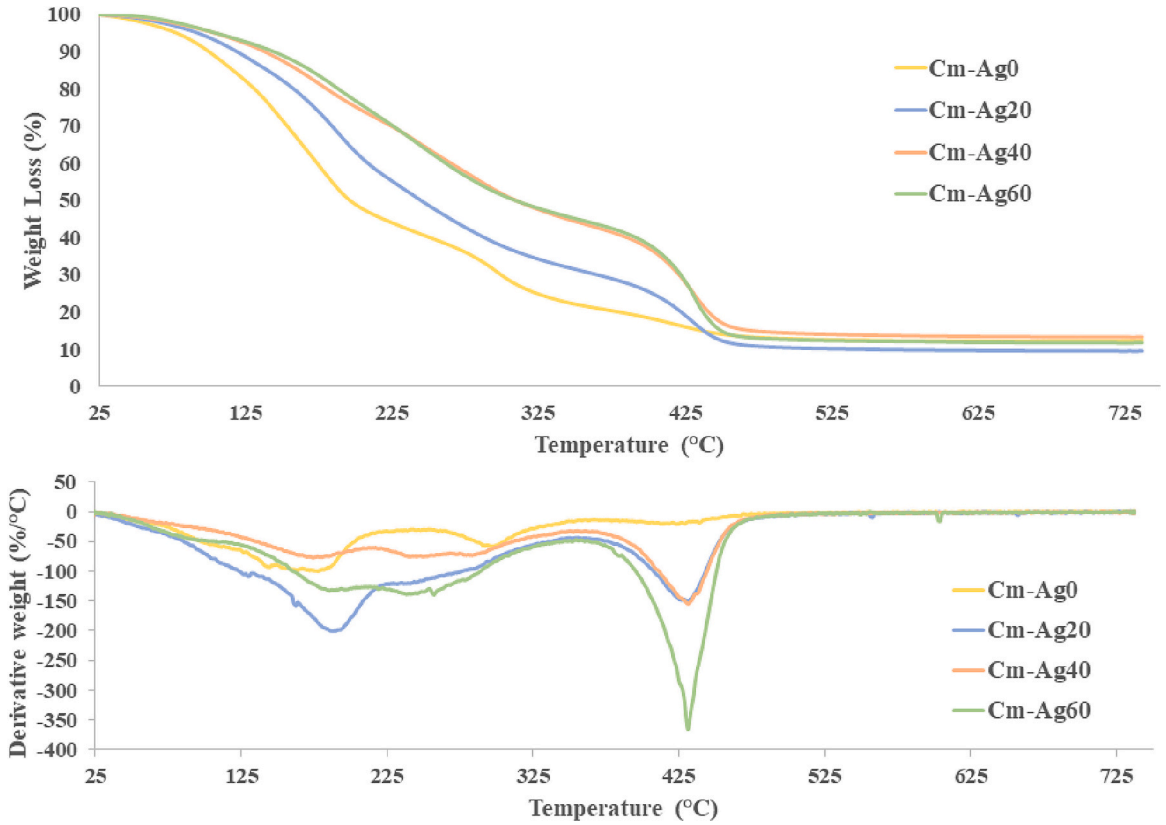

Fig. 8. Thermal properties of biocompatible films.

Table 3
Antibacterial properties of biocompatible films.

	Staphylococcus aureus (ATCC 25923) (mm)	*Pseudomonas aeruginosa* (ATCC 27853) (mm)	*Escherichia coli* (ATCC 25922) (mm)
Cm-Ag0	–	–	–
Cm-Ag20	10.0 ± 1.4	11.5 ± 2.1	13 ± 2.8
Cm-Ag40	14.0 ± 1.4	14.5 ± 0.7	16.0 ± 0.0
Cm-Ag60	16.5 ± 0.7	16.5 ± 2.1	16 ± 1.4
Control			
Ertapenem	31	16	33
Ampicillin	33	–	19
Streptomycin	16	14	16

diffusion method. Test results showed that Ag NPs and CNF/PVA-Ag composite film successfully inhibited the growth of *E. coli* and *B. subtilis*. Inhibition zones of Ag NPs and CNF/PVA-Ag composite film were 10 and 12 mm against *E. coli* and 15 and 17 mm against *B. subtilis*. These results stated that the films synthesized for Gram-negative bacteria were more effective [48]. The same case was seen in the biocompatible films prepared in the present study. The possible cause of bacterial toxicity caused by Ag NPs was due to the release of Ag^+ ions, which then penetrated the bacterial cell membrane. Morones et al. investigated the bactericidal effects of Ag nanoparticles on *E. coli*, *P. aeruginosa*, and *Salmonella* species. The researchers have reported that Ag NPs adhered to the cell membrane and disrupted membrane integrity [49]. In another study, Hsueh et al. reported the toxicity of Ag-NPs against *B. subtilis*, mediated by the release of Ag^+ ions from Ag NPs, which penetrate bacterial cells and then oxidize to Ag_2O inside the cell. Also, it was seen that the hydroxyethyl cellulose acrylate/pentaerythritol tetrakis (3-mercaptopropionate) (Cm-Ag0) matrix did not show

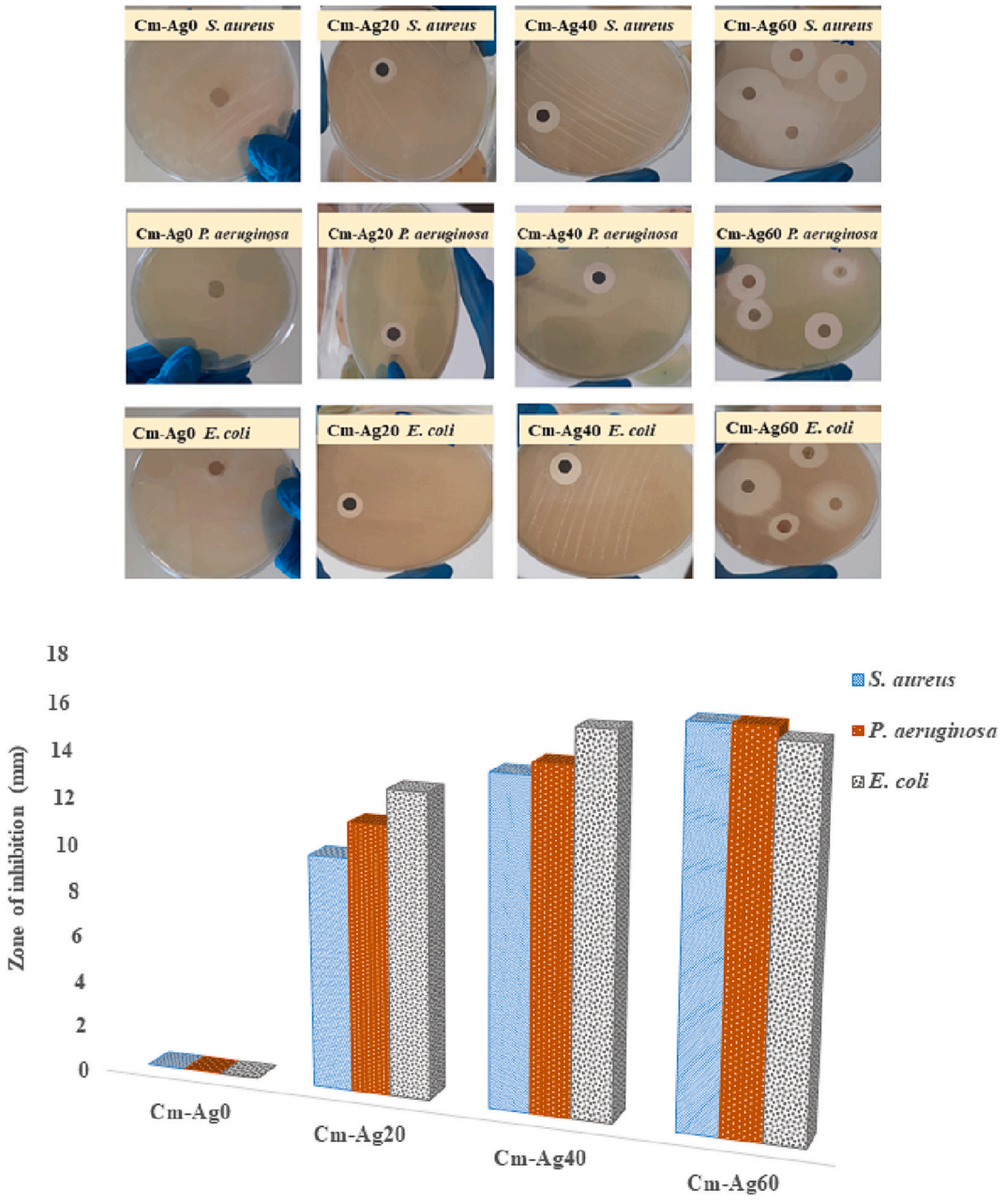

Fig. 9. Antibacterial properties of biocompatible films.

antibacterial activity in all three bacterial species [50]. However, the incorporation of m-Ag NPs into the hydroxyethyl cellulose acrylate/pentaerythritol tetrakis (3-mercaptopropionate) matrix gave them the ability to inhibit the growth of *E. coli*, *P. aeruginosa*, and *S. aureus* in their immediate environment. It can be argued that the addition of m-Ag NPs to the hydroxyethyl cellulose acrylate/pentaerythritol tetrakis (3-mercaptopropionate) matrix makes the prepared film formulations a potential antibacterial agent and can be used for biomedical applications.

In another study in the literature, cellulose nanocrystal/Ag NPs composites with high Ag percentages were obtained by using dialdehyde cellulose nanocrystal (DACNC) as both a reducing and stabilizing agent. The antibacterial activity of the prepared composites against *E. coli* and *S. aureus* was determined using the zone of inhibition method. CNC-AgNPs composites have been reported to develop significant inhibition zones with a 2–8 diameter against both bacteria. No inhibition rings were observed for DACNC as a control, indicating that the antimicrobial activity of CNC-AgNPs was associated with the presence of Ag NPs rather than the CNC itself [51]. The absence of an inhibition zone in the Cm-Ag0 formulation prepared in the present study was consistent with the literature. Dong and Li proposed a simple approach to synthesize a new coating containing chitosan-dialdehyde cellulose nanocrystals and Ag NPs. The antibacterial activity of CS-DCNC-AgNPs was investigated by the disk diffusion test against 1 Gram-negative bacteria, 5 Gram-positive bacteria, and three fungal species. *S. aureus* inhibition zone diameter of CS-DCNC-AgNPs was measured as 8.13. Similarly, the diameters of the inhibition zone of CS-DCNC-AgNPs (10 %), Gram-negative bacteria: *E. coli* (6.96 mm), *P. aeruginosa* (7.45 mm), *K. pneumoniae* (6.90 mm) and *E. cloacae* (10.48 mm). Also, the diameters of the inhibition zone of the three fungi were found as follows: *Candida albicans* (6.41 mm), *Candida glabrata* (7.19 mm), and *Candida krusei* (5.89 mm). Examining all the results, it was found that CS-DCNC-AgNPs showed moderate antibacterial activity [52]. Compared to the studies in the literature, it was seen that the inhibition areas of the films prepared in this study were substantially wider.

3.6. The effect of biocompatible films on cancer cell

The anticancer activity of hydroxyethyl cellulose acrylate/pentaerythritol tetrakis (3-mercaptopropionate) with varying concentrations of m-Ag NPs was tested under *in vitro* conditions against human MCF-7 and VERO cell lines, and the cell viability % values and cytotoxicity potential are shown in Fig. 10 and Supplementary Table 1. (% Cell viability value = test absorbance value / control absorbance value mean × 100). The sensitivity of VERO cells and MCF-7 cells to the prepared films showed significant activity depending on the dose. As seen in Fig. 10, the cell viability of the m-Ag NPs decreases with increasing concentration in the formulation of m-Ag NPs. The decreased cell viability values may be due to the higher chemical content that causes cell damage through processes such as binding and reacting with proteins, phagocytosis, deposition, clearance, and translocation [52]. These results indicated the cytotoxic effect of the prepared films on MCF-7 and argued to be highly lethal for MCF-7 cells. It is also seen in Fig. 10 that all film formulations had no cytotoxic effects on healthy cells. This is a significant result that can prevent the death of normal cells such as hematopoietic and immune cells, and cancer cells due to the many side effects of traditional anticancer agents. The present study used VERO as a normal cell to evaluate undesirable side effects. Prepared biocompatible squids respond to the search for a material with minimal cytotoxic effect against healthy cells and maximum cytotoxic effect against cancer cells.

The results obtained in the study were also related to the m-Ag NPs content of the films. In a study conducted in 2017, it was reported that Ag NPs at concentrations in the range of 0.5–2.5 μg/mL showed significant cytotoxic activity in the MCF-7 cell line. It was determined that Ag NPs (50–400 μg/mL) obtained from *Commelina nudiflora* L. decreased cell viability and showed cytotoxic activity in HCT-116 colon cancer cells [53]. In another study, the possibility of using Ag NPs as drug carriers together with the anticancer drug doxorubicin was investigated, and the results showed that Ag NPs could increase the intracellular concentration of doxorubicin in leukemia K562 cells, hence enhancing its cytotoxic effect on leukemia K562 cells [54]. In a study conducted in 2019, Au-AgNPs from *Trapa natans* effectively induced cytotoxicity in various cancer cells (HCT116, MDA-MB-231 ve HeLa) at a concentration of 200 μg/mL. Cancer cells exposed to Au-AgNPs exhibited apoptotic features such as nuclear condensation, loss of mitochondrial membrane potential, and segmentation of casp-3 and poly(ADP-ribose) polymerase-1 [55]. In a recent study, Ag NPs at a concentration of 100 μg/mL showed a cytotoxicity rate of 40 phr in MCF-7 cells and had almost no cytotoxic effect on VERO cells. Regarding the phenotypic apoptotic (programmed cell death) changes analyzed using acridine orange, eosin, and hematoxylin, Ag NPs caused apoptosis and vacuole degeneration as well as the emergence of necrotic in MCF-7 cells. In contrast, in the normal cell line VERO, any phenotypic did not cause apoptotic changes [56]. In another study, the cytotoxicity of the HEC hydrogel against MCF-7 cells was examined by the MTT test and the cell viability value was calculated as 29.8 ± 4.9 % [57]. Examining the results of these studies, it was seen that the cell viability value of the Cm-Ag60 material, of which its cytotoxicity was examined in the MCF-7, was 4.424 ± 8.852 %. Comparing the results to those reported in the previous studies, it was seen that the lethality against cancer cells was superior. All these studies suggest the anticancer activity of Ag NPs. It was seen that the

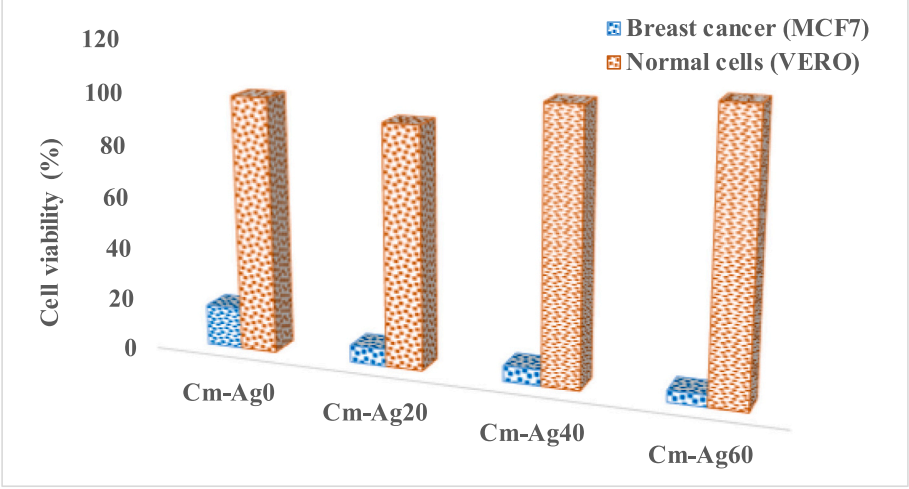

Fig. 10. Evaluation of the effects of the prepared films on healthy cells and breast cancer cells.

films prepared in the cytotoxicity test obtained in the present study were selective in killing cancerous cells and did not cause any inhibition in healthy cells. The reason for this is that silver nanoparticles have high activity thanks to their great surface/volume ratios and can easily enter cells, interact with cell components, and thus disrupt cellular signaling pathways. It has been previously reported in the literature that AgNPs interact with mitochondria and disrupt cellular electron transfer chain activity, resulting in an increase in reactive oxygen species (ROS) levels [58]. It has been suggested that the increased cytotoxicity of AgNPs against cancerous cells is owing to their higher nanoparticle uptake by these cells rather than healthy cells, given that cancerous cells have an irregular metabolism and fast proliferation rate, thus making them more vulnerable [59,60]. These results pave the way for the formulations produced to be considered a drug delivery system for a known cancer drug in different forms.

4. Conclusion

Ag NPs and HEC, of which the surface was modified with acrylate groups, were successfully synthesized, and FTIR characterized their structures. The synthesized m-Ag NPs were added to formulations containing 0, 20, 40, and 60 phr, HEC with acrylate functionality, 4-SH, a photoinitiator, and biocompatible films were made prepared practically by the thiol-ene click reaction. SEM examined the morphological properties of the prepared films, and it was observed that Ag NPs were homogeneously distributed on the surface. Also, their elemental composition was characterized by SEM-EDAX, and peaks of Ag and Si elements were observed in other films (Cm-Ag20, Cm-Ag40, and Cm-Ag60) compared to films with no Ag NPs (Cm-Ag0). The antibacterial effect of the films was evaluated by disk diffusion test against *E. coli*, *P. aeruginosa*, and *S. aureus*. The Cm-Ag0 control formulation did not form an inhibition zone in three bacteria. It was observed that the increased levels of m-Ag NPs in the formulations increased the area of inhibition against bacteria. It was found that all prepared films showed good antibacterial properties against *E. coli*, *P. aeruginosa*, and *S. aureus*. It was observed that the film with the Cm-Ag60 formulation had a better antibacterial effect in three bacteria than the Streptomycin antibiotic used for the control. The MTT test against live and breast cancer cell lines examined the prepared films' cell viability values and cytotoxicity potentials. It was observed that materials with minimum cytotoxic effect against healthy cells and maximum cytotoxic effect against cancer cells were prepared for use in cancer treatment. The film materials prepared and examined for their properties can be used effectively for many pharmaceutical and food industry applications. In addition, UV-curable coatings with high biocompatibility and low cytotoxicity provide a functional coating for stents in the clinic.

Funding

This work was supported by Amasya University, Commission of Scientific Research Project under grant FMB-BAP 20-0460.

CRediT authorship contribution statement

Acquisition of data: Yusuf Özdemir, Hatice Birtane, Aslı Beyler-Çigil.

Analysis and/or interpretation of data: Yusuf Özdemir, Hatice Birtane, Aslı Beyler-Çigil.

Drafting the manuscript: Aslı Beyler-Çigil.

Revising the manuscript critically for important intellectual content: Yusuf Özdemir, Hatice Birtane, Aslı Beyler-Çiğil.

Approval of the version of the manuscript to be published: Yusuf Ozdemir, Hatice Birtane, Aslı Beyler-Çigil.

Declaration of competing interest

The authors declare that they have no known competing financial interests or personal relationships that could have appeared to influence the work reported in this paper.

Appendix A. Supplementary data

Supplementary data to this article can be found online at https://doi.org/10.1016/j.ijbiomac.2023.125516.

References

[1] P. Anand, A.B. Kunnumakkara, C. Sundaram, K.B. Harikumar, S.T. Tharakan, O. S. Lai, B. Sung, B.B. Aggarwal, Cancer is a preventable disease that requires major lifestyle changes, Pharm. Res. 25 (9) (2008) 2097–2213.
[2] H. Danafar, A.H. Taromchi, A. Rakhshbahar, A. Sharafi, V. Hasani, S. Tafvizi, M. Rostami, Co-delivery of methotrexate and curcumin with mPEG-PCL polymeric nanoparticles and evaluation of toxicity effect on MCF7 breast cancer cell line, Inorg. Chem. Commun. 142 (2022), 109715.
[3] J.L. Khatcheressian, P. Hurley, E. Bantug, L.J. Esserman, E. Grunfeld, F. Halberg, A. Hantel, N.L. Henry, H.B. Muss, T.J. Smith, V.G. Vogel, A.C. Wolff, M. R. Somerfield, N.E. Davidson, Breast cancer follow-up and management after primary treatment: American Society of Clinical Oncology clinical practice guideline update, Proc. Am. Soc. Clin. Oncol. 31 (2013) 961–966.
[4] M. Cloutier, D. Mantovani, F. Rosei, Antibacterial coatings: challenges, perspectives, and opportunities, Trends Biotechnol. 33 (2015) 637–652.
[5] Vy.T.H. Pham, C.M. Bhadra, V.K. Truong, R.J. Crawford, E.P. Ivanova, Designing antibacterial surfaces for biomedical implants, Antibacterial Surf. 1072 (2015) 89–111.
[6] M. Terreni, M. Taccani, M. Pregnolato, New antibiotics for multidrug-resistant bacterial strains: latest research developments and future perspectives, Molecules 26 (2021) 2671.
[7] Q.-Y. Chen, S.-L. Xiao, S.Q. Shi, L.-P. Cai, A one-pot synthesis and characterization of antibacterial silver nanoparticle–cellulose film, Polymers 12 (2020) 440.
[8] C. Marambio-Jones, E.M.V. Hoek, A review of the antibacterial effects of silver nanomaterials and potential implications for human health and the environment, J. Nanopart. Res. 12 (2010) 1531–1551.
[9] Y.-G. Yuan, Q.-L. Peng, S. Gurunathan, Effects of silver nanoparticles on multiple drug-resistant strains of Staphylococcus aureus and Pseudomonas aeruginosa from mastitis-infected goats: an alternative approach for antimicrobial therapy, Int. J. Mol. Sci. 18 (2017) 569.
[10] N. Durán, M. Durán, M.B. de Jesus, A.B. Seabra, W.J. Fávaro, G. Nakazato, Silver nanoparticles: a new view on mechanistic aspects on antimicrobial activity, Nanomedicine 12 (2016) 789–799.
[11] A.J. Kora, R.B. Sashidharb, Biogenic silver nanoparticles synthesized with rhamnogalacturonan gum: antibacterial activity, cytotoxicity and its mode of action, Arab. J. Chem. 11 (2018) 313–323.
[12] W.-R. Li, X.-B. Xie, Q.-S. Shi, H.-Y. Zeng, Y.-S. Ou-Yang, Y.-B. Chen, Antibacterial activity and mechanism of silver nanoparticles on *Escherichia coli*, Appl. Microbiol. Biotechnol. 85 (2009) 1115–1122.
[13] C.A. Arenas-Chávez, L.M. de Hollanda, A.A. Arce-Esquivel, A. Alvarez-Risco, S. Del-Aguila-Arcentales, J.A. Yáñez, C. Vera-Gonzales, Antibacterial and antifungal activity of functionalized cotton fabric with nanocomposite based on silver nanoparticles and carboxymethyl chitosan, Processes 10 (2022) 1088.
[14] A. Ghazizadeh, S.A. Haddadi, M. Mahdavian, The effect of sol-gel surface modified silver nanoparticles on the protective properties of the epoxy coating, RSC Adv. 6 (2016) 18996–19006.
[15] M. Kawashita, S. Tsuneyama, F. Miyaji, T. Kokubo, H. Kozuka, K. Yamamoto, Antibacterial silver-containing silica glass prepared by sol-gel method, Biomaterials 21 (2000) 393–398.
[16] A.A. Issa, A.S. Luyt, Kinetics of alkoxysilanes and organoalkoxysilanes polymerization: a review, Polymers 11 (2019) 537.
[17] R. Rajan, E. Rainosalo, S.P. Thomas, S.K. Ramamoorthy, J. Zavašnik, J. Vuorinen, M. Skrifvars, Modification of epoxy resin by silane-coupling agent to improve tensile properties of viscose fabric composites, Polym. Bull. 75 (2018) 167–195.
[18] K. Wieszczycka, K. Staszak, M.J. Woźniak-Budych, J. Litowczenko, B. M. Maciejewska, S. Jurga, Surface functionalization – the way for advanced applications of smart materials, Coord. Chem. Rev. 436 (2021), 213846.
[19] A. Ozcan, A. Tozluoglu, E. Arman-Kandirmaz, A. Tutus, H. Fidan, Printability of variative nanocellulose derived papers, Cellulose 28 (2021) 5019–5031.
[20] F. Wang, J.D. Harindintwali, Z. Yuan, M. Wang, F. Wang, S. Li, Z. Yin, L. Huang, Y. Fu, L. Li, S.X. Chang, L. Zhang, J. Rinklebe, Z. Yuan, Q. Zhu, L. Xiang, D.C. W. Tsang, L. Xu, X. Jiang, J. Liu, N. Wei, M. Kästner, Y. Zou, Y.S. Ok, J. Shen, D. Peng, W. Zhang, D. Barceló, Y. Zhou, Z. Bai, B. Li, B. Zhang, K. Wei, H. Cao, Z. Tan, L.b. Zhao, X. He, J. Zheng, N. Bolan, X. Liu, C. Huang, S. Dietmann, M. Luo, N. Sun, J. Gong, Y. Gong, F. Brahushi, T. Zhang, C. Xiao, X. Li, W. Chen, N. Jiao, J. Lehmann, Y.-G. Zhu, H. Jin, A. Schäffer, J.M. Tiedje, J.M. Chen, Technologies and perspectives for achieving carbon neutrality, Inovation 2 (2021), 100180.
[21] M. Oprea, S.I. Voicu, Recent advances in composites based on cellulose derivatives for biomedical applications, Carbohydr. Polym. 247 (2020), 116683.
[22] A. Samir, F.H. Ashour, A.A.A. Hakim, M. Bassyouni, Recent advances in biodegradable polymers for sustainable applications, npj Mater. Degrad. 6 (2022) 68.

[23] H. Seddiqi, E. Oliaei, H. Honarkar, J. Jin, L.C. Geonzon, R.G. Bacabac, J. Klein-Nulend, Cellulose and its derivatives: towards biomedical applications, Cellulose 28 (2021) 1893–1931.
[24] J.O. Echavarría, N.A.G. Vanegas, C.P.O. Orozco, Chitosan/carboxymethyl cellulose wound dressings supplemented with biologically synthesized silver nanoparticles from the ligninolytic fungus anamorphous *Bjerkandera* sp. R1, Heliyon 8 (2022) 10258.
[25] Y. He, H. Li, X. Fei, L. Peng, Carboxymethyl cellulose/cellulose nanocrystals immobilized silver nanoparticles as an effective coating to improve barrier and antibacterial properties of paper for food packaging applications, Carbohydr. Polym. 252 (2021), 117156.
[26] H. Jia, X. Zeng, S. Fan, R. Cai, Z. Wang, Y. Yuan, T. Yue, Silver nanoparticles anchored magnetic self-assembled carboxymethyl cellulose-ε-polylysine hybrids with synergetic antibacterial activity for wound infection therapy, Int. J. Biol. Macromol. 210 (2022) 703–715.
[27] A. Beyler-Çiğil, F. Şen, H. Birtane, M.V. Kahraman, Covalently bonded nanosilver-hydroxyethyl cellulose/polyacrylic acid/sorbitol hybrid matrix: thermal, morphological and antibacterial properties, Polym. Bull. 79 (2022) 11353–11368.
[28] A.B. Lowe, Thiol-ene "click" reactions and recent applications in polymer and materials synthesis, Polym. Chem. 1 (2010) 17–36.
[29] Y. Zhang, S. Liu, T. Li, L. Zhang, U. Azhar, J. Ma, C. Zhai, C. Zong, S. Zhang, Cytocompatible and non-fouling zwitterionic hyaluronic acid-based hydrogels using thiol-ene "click" chemistry for cell encapsulation, Carbohydr. Polym. 236 (2020), 116021.
[30] M. Black, J.W. Rawlins, Thiol–ene UV-curable coatings using vegetable oil macromonomers, Eur. Polym. J. 45 (2009) 1433–1441.
[31] H. Durand, I. Baussanne, M. Demeunynck, J. Viger-Gravel, L. Emsley, M. Bardet, E. Zeno, N. Belgacem, J. Bras, Two-step immobilization of metronidazole prodrug on TEMPO cellulose nanofibrils through thiol-yne click chemistry for in situ controlled release, Carbohydr. Polym. 262 (2021), 117952.
[32] S. Lee, H. Tae, C.S. Ki, Fabrication of schizophyllan hydrogel via orthogonal thiol-ene photopolymerization, Carbohydr. Polym. 167 (2017) 270–279.
[33] H. Birtane, F. Şen, B. Bozdağ, M.V. Kahraman, Antibacterial UV-photocured acrylic coatings containing quaternary ammonium salt, Polym. Bull. 78 (2021) 3577–3588.
[34] Z. Lu, J. Huang, E. Songfeng, J. Li, L. Si, C. Yao, F. Jia, M. Zhang, All cellulose composites prepared by hydroxyethyl cellulose and cellulose nanocrystals through the crosslink of polyisocyanate, Carbohydr. Polym. 250 (2020), 116919.
[35] F. Ahangaran, A.H. Navarchian, Recent advances in chemical surface modification of metal oxide nanoparticles with silane coupling agents: a review, Adv. Colloid Interf. Sci. 286 (2020), 102298.
[36] S. Maharjan, K.-S. Liaoa, A.J. Wang, Z. Zhu, B.P. McElhenny, J. Bao, S.A. Curran, Synthesis of stabilized silver nanoparticles in organosiloxane matrix via sol-gel method and its optical nonlinearity study, Chem. Phys. 532 (2020), 110610.
[37] L. Milliere, K. Makasheva, C. Laurent, B. Despax, L. Boudou, G. Teyssedre, Silver nanoparticles as a key feature of a plasma polymer composite layer in mitigation of charge injection into polyethylene under dc stress, J. Phys. D. Appl. Phys. 49 (2016), 015304.
[38] L. Song, J. Chen, Y. Bian, L. Zhu, Y. Zhou, Y. Xiang, D. Xia, Synthesis, characterization and desulfurization performance of MCM-41 functionalized with Cu by direct synthesis and organosilanes by grafting, J. Porous. Mater. 22 (2015) 379–385.
[39] K. Chandraker, S.K. Vaishanav, R. Nagwanshi, M.L. Satnami, Radical scavenging efficacy of thiol capped silver nanoparticles, J. Chem. Sci. 127 (2015) 2183–2191.
[40] E. Effati, B. Pourabbas, One-pot synthesis of sub-50 nm vinyl- and acrylate-modified silica nanoparticles, Powder Technol. 219 (2012) 276–283.
[41] S. Das, K. Bandyopadhyay, M.M. Ghosh, Effect of stabilizer concentration on the size of silver nanoparticles synthesized through chemical route, Inorg. Chem. Commun. 123 (2021), 108319.
[42] B.R. Khalkho, R. Kurrey, M.K. Deb, K. Shrivas, S.S. Thakur, S. Pervez, V.K. Jain, L-cysteine modified silver nanoparticles for selective and sensitive colorimetric detection of vitamin B1 in food and water samples, Heliyon 6 (2020) 03423.
[43] S.M. Solyman, M.S.A. Darwish, J. Yoon, Catalytic activity of hybrid Iron oxide silver nanoparticles in methyl methacrylate polymerization, Catalysts 10 (2020) 422.
[44] M. Akbarian, M.E. Olya, M. Ataeefard, M. Mahdavian, The influence of nanosilver on thermal and antibacterial properties of a 2 K waterborne polyurethane coating, Prog. Org. Coat. 75 (2012) 344–348.
[45] M.J. Palimi, M. Rostami, M. Mahdavian, B. Ramezanzadeh, Surface modification of Cr_2O_3 nanoparticles with 3-amino propyl trimethoxy silane (APTMS). Part 1: studying the mechanical properties of polyurethane/Cr_2O_3 nanocomposites, Prog. Org. Coat. 77 (2014) 1663–1673.
[46] G.F.E. Fawal, M.M. Abu-Serie, M.A. Hassan, M.S. Elnouby, Hydroxyethyl cellulose hydrogel for wound dressing: fabrication, characterization and in vitro evaluation, Int. J. Biol. Macromol. 111 (2018) 649–659.
[47] A. Ali, I.U. Haq, J. Akhtar, M. Sher, N. Ahmed, M. Zia, Synthesis of Ag-NPs impregnated cellulose composite material: its possible role in wound healing and photocatalysis, IET Nanobiotechnol. 11 (2017) 477–484.
[48] M.V. Limaye, V. Gupta, S.B. Singh, G.R. Paik, P. Singh, Antimicrobial activity of composite consisting of cellulose nanofibers and silver nanoparticles, ChemistrySelect 4 (2019) 12164–12169.
[49] J.R. Morones, J.L. Elechiguerra, A. Camacho, K. Holt, J.B. Kouri, J.T. Ramírez, M. J. Yacaman, The bactericidal effect of silver nanoparticles, Nanotechnology 16 (2005) 2346.
[50] Y.-H. Hsueh, K.-S. Lin, W.-J. Ke, C.-T. Hsieh, C.-L. Chiang, D.-Y. Tzou, S.-T. Liu, The antimicrobial properties of silver nanoparticles in *Bacillus subtilis* are mediated by released Ag+ ions, PLoS One 10 (2015), 0144306.
[51] Q. Xu, L. Jin, Y. Wang, H. Chen, M. Qin, Synthesis of silver nanoparticles using dialdehyde cellulose nanocrystal as a multi-functional agent and application to antibacterial paper, Cellulose 26 (2018) 1309–1321.
[52] F. Dong, S. Li, Wound dressings based on chitosan-dialdehyde cellulose nanocrystals-silver nanoparticles: mechanical strength, antibacterial activity and cytotoxicity, Polymers 10 (2018) 673.
[53] P. Kuppusamy, S.J.A. Ichwan, P.N.H. Al-Zikri, W.H. Suriyah, I. Soundharrajan, N. Govindan, G.P. Maniam, M.M. Yusoff, In vitro anticancer activity of Au, Ag nanoparticles synthesized using *Commelina nudiflora* L. aqueous extract against HCT-116 colon cancer cells, Biol. Trace Elem. Res. 173 (2016) 297–305.
[54] D. Guo, Y. Zhao, Y. Zhang, Q. Wang, Z. Huang, Q. Ding, Z. Guo, X. Zhou, L. Zhu, N. Gu, The cellular uptake and cytotoxic effect of silver nanoparticles on chronic myeloid leukemia cells, J. Biomed. Nanotechnol. 10 (2014) 669–678.
[55] N. Ahmad, A.K. Sharma, S. Sharma, I. Khan, D.K. Sharma, A. Shamsi, T.R.S. Kumar, M. Seervi, Biosynthesized composites of Au-Ag nanoparticles using Trapa peel extract induced ROS mediated p53 independent apoptosis in cancer cells, Drug Chem. Toxicol. 42 (2019) 43–53.
[56] M.H. Sangour, I.M. Ali, Z.W. Atwan, A.A.A.L.A.A. Ali, Effect of Ag nanoparticles on viability of MCF-7 and Vero cell lines and gene expression of apoptotic genes, Egypt. J. Med. Hum. Genet. 22 (2021) 9.
[57] N.S. El-Sayed, H. Awad, G.M. El-Sayed, Z.A. Nagieb, S. Kamel, Synthesis and characterization of biocompatible hydrogel based on hydroxyethyl cellulose-g-poly (hydroxyethyl methacrylate), Polym. Bull. 77 (2020) 6333–6347.
[58] R.A. Cairns, I.S. Harris, T.W. Mak, Regulation of cancer cell metabolism, Nat. Rev. Cancer 11 (2011) 85–95.
[59] S. Khorrami, A. Zarrabi, M. Khaleghi, M. Danaei, M.R. Mozafari, Selective cytotoxicity of green synthesized silver nanoparticles against the McF-7 tumor cell line and their enhanced antioxidant and antimicrobial properties, Int. J. Nanomedicine 13 (2018) 8013–8024.
[60] R.P. Singh, P. Ramarao, Cellular uptake, intracellular trafficking and cytotoxicity of silver nanoparticles, Toxicol. Lett. 213 (2012) 249–259.